Journal of Power Sources 210 (2012) 366–373

Contents lists available at SciVerse ScienceDirect

Journal of Power Sources

journal homepage: www.elsevier.com/locate/jpowsour

Long-term cell degradation mechanism in high-temperature proton exchange membrane fuel cells

Yuka Oono[a,*], Atsuo Sounai[b], Michio Hori[a]

[a] Fuel Cell Research Center, Daido University, 10-3 Takiharu-cho, Minami-ku, Nagoya, Aichi 457-8530, Japan
[b] Dept. of Materials Science & Engineering, Suzuka National College of Technology, Shirako-cho, Suzuka, Mie 510-0294, Japan

ARTICLE INFO

Article history:
Received 7 December 2011
Received in revised form 20 February 2012
Accepted 23 February 2012
Available online 24 March 2012

Keywords:
High-temperature proton exchange membrane fuel cells
Performance
Durability
Polybenzimidazole
Phosphoric acid
Mechanism

ABSTRACT

The mechanism underlying the decline in cell voltage over time was investigated for high-temperature proton exchange membrane fuel cells. Five identical cells were prepared and long-term power generation tests were conducted at an operation temperature of 150 °C and a current density of 0.2 A cm^{-2} for periods of up to 17,860 h. Each of the cells was then analyzed using transmission electron microscopy and electron probe micro-analysis (EPMA). The results indicated that growth of the Pt catalyst particles occurred during operation, in addition to oxidation of the carbon support. Degradation of the catalyst layers was investigated by EPMA of cross sections of the membrane electrode assemblies, allowing the mechanism of cell performance reduction to be clarified.

© 2012 Elsevier B.V. All rights reserved.

1. Introduction

Fuel cells have attracted attention as an environmentally friendly, clean energy source and have been the subject of a large amount of research. At present, the most actively studied fuel cell is the perfluorosulfonic acid-type low-temperature proton exchange membrane fuel cell (LT-PEMFC). The LT-PEMFC is different from previous generation fuel cells in that it uses a solid polymer membrane as the electrolyte, with water as the proton conduction medium, and can therefore operate at temperatures below 100 °C. Consequently, the LT-PEMFC has widened the range of applications of fuel cells to include small-scale power sources for automobiles, homes and portable devices, and such applications are expected to expand in the future. A recent trend in Japan is the commercialization of 1-kW class domestic cogeneration systems that use both electricity and electrically generated waste heat, due to significant improvements in fuel cell performance and durability [1]. However, a major stumbling block for commercialization is that such systems tend to be very complex and expensive, because LT-PEMFCs inherently require humidification for proton conduction via water. In addition, system efficiency is relatively low due to the low operating temperature of <100 °C [1], and a CO selective oxidizer is required since the CO tolerance of the electrode catalyst is reduced at low temperature [2–4].

Research on the next generation of PEMFCs is currently underway, and it is hoped that these problems can be resolved by simplification of the system, reduction of the production cost, and improvement of the efficiency at operating temperatures of 150–200 °C [5]. An additional requirement is that the PEMFCs have sufficient high temperature tolerance in the absence of humidification, and be based on polymer electrolytic membranes that can be chemically coupled with acids capable of proton conduction. To this end, research has been carried out on acids that are capable of proton conduction at temperatures above 100 °C, in addition to acid-absorbing polymers [6–8]. The results suggest that sulfuric and phosphoric acids have a high proton conduction capability [9]. With regard to the polymers used for the membranes, fundamental studies have been carried out on polybenzimidazole (PBI) [10], polyethylene oxide (PEO) [11], polyvinyl alcohol (PVA) [12,13], polyacrylamide (PAAM) [14] and polyethylenimine (PEI) [15].

Investigations have been carried out on HT-PEMFCs based on phosphoric-acid-doped PBI membranes, from the viewpoint of not only the membrane conductivity and heat resistance [16,17], but also the power generation capability of actual cells [18–22]. Zhang et al. reported that higher cell performance was achieved as the operating temperature approached 200 °C [22]. In addition, lifetimes exceeding 10,000 h have been reported by research groups at BASF and Samsung [23,24], and these PEMFCs are considered to be closest to commercial viability.

* Corresponding author. Tel.: +81 52 612 6111x5621; fax: +81 52 612 5623.
E-mail address: oono-y@daido-it.ac.jp (Y. Oono).

0378-7753/$ – see front matter © 2012 Elsevier B.V. All rights reserved.
doi:10.1016/j.jpowsour.2012.02.098

However, there have been very few reports on the mechanism underlying the deterioration of such cells. Although some studies have been carried out on the reduction in durability during 500 h of operation at 150 °C [21], nothing has been reported concerning the causes of cell deterioration over longer periods.

In the present study, in order to clarify the causes of long-term cell deterioration, five identical cells were tested for periods of up to 17,860 h, and their membrane electrode assemblies (MEAs) were then removed and subjected to microstructural analysis. The cells used PBI membranes doped with phosphoric acid. The deterioration mechanism was investigated based on chronological changes in the cell voltage and internal cell resistance, chronocoulometry (CC) measurements of the hydrogen crossover, and post-analysis using transmission electron microscopy (TEM) and electron probe micro-analysis (EPMA).

2. Experimental

2.1. Preparation of PBI electrolyte membrane

PBI membranes (5.5 cm × 5.5 cm, ca. 40 μm thick) provided by the joint research institute were immersed in an 85% phosphoric acid solution and heated to 40 °C for 40 min to dope the membranes [25]. All of the membranes used in the present study were subjected to exactly the same doping procedure. The doping level was determined by measuring the weights of the membranes before and after doping using a precision electronic balance (AUW120D, Shimadzu Corp., Japan); this was characterized by the ratio of the weight of phosphoric acid doped into the membrane to the weight of the membrane after doping with phosphoric acid.

2.2. Production of electrodes

A sheet of carbon paper with a thickness of 280 μm (TGP-H-090, Toray Corp., Japan) was used as the gas diffusion layer. A mixed powder of Ketchen Black (EC-600JD, Akzo Nobel Corp., UK) and polytetrafluoroethylene (PTFE, DuPont) in a weight ratio of 65:35 was applied to the carbon paper using a dry coating device [25–28] until it formed a coating with a density of 2 mg cm^{-2}. This was then heated at 350 °C in an atmospheric oven, and the surface was leveled using a roller press [25–28] to produce a filled carbon layer.

A catalyst ink was then prepared by mixing polyvinylidene fluoride (PVDF, Kureha Corp., Japan), Pt-supported and PtCo-supported on Ketchen Black powder (carbon/metal: 50/50, TKK Corp., Japan) [25] and N-methyl pyrrolidone (NMP, Sigma–Aldrich Corp., USA) with agitation for 60 h. To produce the electrode, the catalyst ink was applied using a wet-coating method onto carbon paper coated with a mixed powder of carbon and PTFE prepared using a dry-coating method. The resulting structure was then dried for 1 h at 80 °C in air, and finally held in a vacuum oven at 160 °C for 25 h to remove the NMP [25]. The amount of supported Pt was approximately 0.8 mg cm^{-2} for both the anode and cathode electrodes.

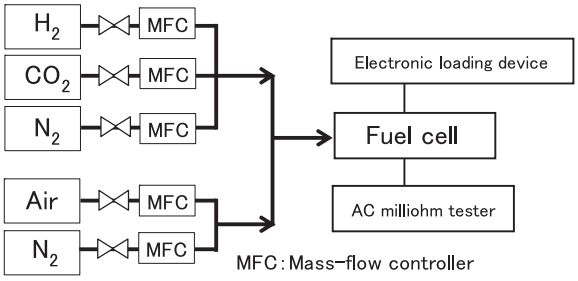

Fig. 1. Schematic diagram of the fuel cell station used in this study.

2.3. Single cell assembly

The electrolyte membrane doped with phosphoric acid was sandwiched between two electrodes prepared as described in Section 2.2 to produce the MEA. This was in turn sandwiched between current collector and bi-polar plates made of carbon, on which a serpentine flow pattern was machined. The flow pattern was designed by the Japan Automobile Research Institute and had a reaction area of 5 cm × 5 cm. This assembly was further sandwiched between a pair of stainless steel end plates with a rubber heater attached to their outermost surfaces and tightened using eight M6 bolts to produce a single cell [25]. Five single cells were prepared, and these are referred to as Cells A, B, C, D and E.

2.4. Long-term power generation durability tests

The five single cells described in Section 2.3 were mounted on a fuel cell station (Kofloc Corp., Japan) equipped with mass-flow controllers, an electronic loading device (Kikusui Electronics Corp., Japan) for controlling the electric current, an AC milliohm tester (Model 3566, Tsuruga Electric Corp., Japan) with a constant frequency of 1 kHz, and a personal computer for equipment monitoring and data output. Fig. 1 shows a schematic diagram of the fuel cell station used in this study.

Table 1 shows the test conditions of Cells A, B, C, D and E. Cell A was used as a reference and did not undergo power generation. It was heated to 150 °C and was kept at that temperature for 5 h while supplying 130 mL min^{-1} (stoich: 3.7) of nitrogen to both the anode and cathode sides. It was then cooled down and its MEA was removed for analysis. Such a stoichiometry was decided by the lowest flow rate limit of the fuel cell station.

For Cells B, C, D and E, power generation tests were conducted at a cell temperature of 150 °C and a current density of 0.2 A cm^{-2}, controlled using an electronic loading device while supplying 130 mL min^{-1} (stoich: 3.7) of pure hydrogen and 310 mL min^{-1} (stoich: 3.7) of air to the anode and cathode sides, respectively. Neither of the reaction gases were humidified [25]. All power generation tests were conducted under atmospheric conditions. For Cells B, C and D, long-term durability tests were conducted for 2000, 12,000, and 15,000 h, respectively, after which power generation was terminated. For Cell E, the long-term durability test was not terminated until the cell voltage had dropped by 10% from its peak value.

Table 1
Test conditions of Cells A, B, C, D and E.

	Cell A	Cell B	Cell C	Cell D	Cell E
Cell temperature	150 °C				
Anode	Nitrogen 130 mL min^{-1}		Hydrogen 130 mL min^{-1}		
Cathode	Nitrogen 130 mL min^{-1}		Air 310 mL min^{-1}		
Current density	–		0.2 A cm^{-2}		
Power generation time (h)	To be kept for 5 h at 150 °C	2000	12,000	15,000	17,800

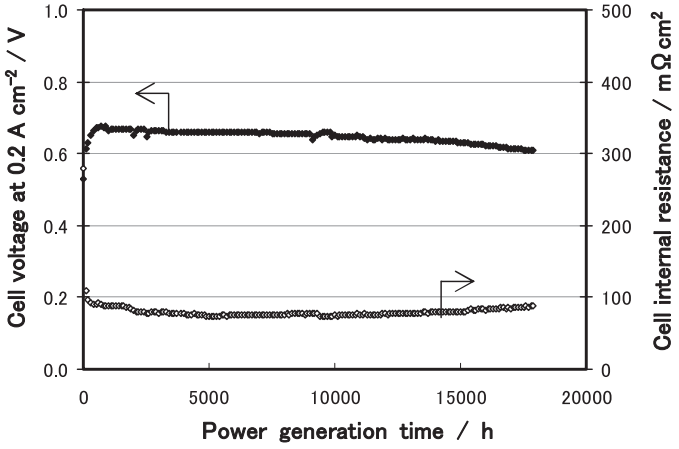

Fig. 2. Long-term power generation test results for Cell E operated until its cell voltage dropped by 10% from it peak value (17,860 h).

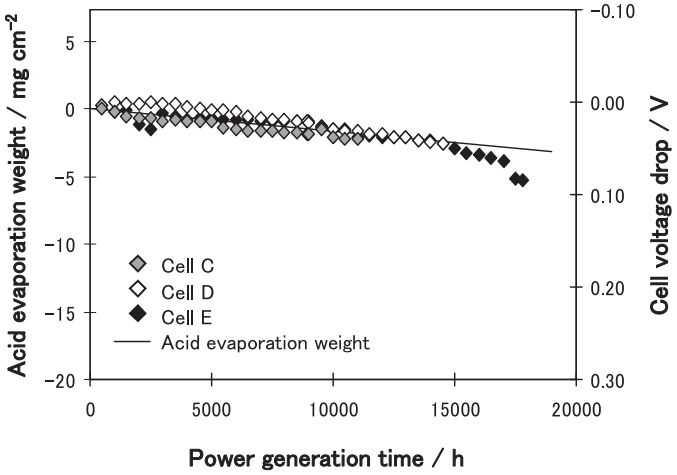

Fig. 3. Long-term power generation test results for Cells B, C, D, and E, operated for 2000, 12,000, 15,000, and 17,860 h, respectively.

During the long-term tests, chronological changes of the cell voltage, internal cell resistance and leak current were monitored. The internal resistance was measured using the above-mentioned AC milliohm tester at a constant frequency of 1 kHz. A potentiostat–galvanostat (HZ-5000 HAG-3001, Hokuto Denko Corp., Japan), was used for CC measurements of the hydrogen crossover rate through the PBI membrane [27]. During the measurements, the cells were operated at 150 °C while providing pure hydrogen to the anode and nitrogen to the cathode. A voltage of 0.2 V was applied across the cell so that hydrogen crossing the membrane was electrochemically oxidized. To measure the hydrogen crossover rate, the hydrogen and nitrogen flow rates were controlled at 300 and 500 mL min^{-1}, respectively.

2.5. Post analyses

TEM (JEM-2010DM, JEOL Ltd. Japan) observations were conducted on the electrode catalysts from both the anode and cathode of Cells A and E, following the tests described in Section 2.4. Cross sections of the MEAs, consisting of the catalyst layer (CL), gas diffusion layer (GDL) and the intermediate microporous layer (MPL) were investigated using EPMA (EPMA-1610, Shimadzu, Japan).

3. Results

3.1. Long-term durability test

Fig. 2 shows the chronological change in the cell voltage and internal resistance during the power generation test conducted on Cell E As described earlier, this test was carried out until the cell voltage decreased by 10% from its peak value, which occurred following 17,860 h of operation. As seen in the figure, the cell voltage initially increased and reached a peak after about 500 h of operation. It then declined very gradually over a period of about 14,000 h with three temporarily drops and recoveries due to emergency stops. It subsequently dropped more rapidly, with a corresponding increase in internal resistance.

In order to investigate the mechanism behind the gradual decrease in performance up to 14,000 h and the subsequent more rapid degradation, power generation tests were carried out on Cells B, C and D for 2000, 12,000, and 15,000 h, respectively. The results are described in the next section.

3.2. Investigation of degradation mechanism

Fig. 3 shows the chronological changes in cell voltage for Cells B, C, D and E. As can be seen, all cells showed a similar drop in voltage until the end of their testing period. In the figure, the solid line represents the loss of phosphoric acid per unit area, calculated based on the amount of evaporation at 150 °C, as described in a previous report [28,29]. The rates of phosphoric acid depletion and cell voltage reduction are in good agreement until around 14,000 h. However, for periods longer than this, a faster dropoff in voltage is seen.

Thus, although it cannot be denied that the depletion of phosphoric acid has a substantial effect on reducing the cell voltage over the entire cell lifetime, another contribution is thought to be an increase in the size of the catalyst particles [21]. To verify this, the MEAs were removed from Cells A and E and the catalysts were analyzed using TEM.

3.3. TEM observations of electrode catalysts

Fig. 4(a) and (b) shows TEM images of the catalysts from the anodes of Cells A and E, respectively, and Fig. 4(c) shows the Pt particle size distributions obtained from these images including Cells C and D. The distributions are seen to be very similar, indicating that very little particle growth occurred in the catalyst of Cell E during 17,860 h of power generation, although there is a slight decrease in the number of small particles.

Fig. 5(a–1) and (b-1) shows TEM images of the catalysts from the cathodes of Cells A and E, respectively, and Fig. 5(c) shows the corresponding particle size distribution. In this case, a significant increase in particle size appears to have occurred in Cell E; the average particle diameters for Cells A and E are 4.6 and 7.9 nm, respectively. In particular, a large decrease in the number of small particles is apparent following 17,860 h of power generation.

Fig. 5(a-2) and (b-2) shows higher magnification TEM images of the regions indicated in Fig. 5(a-1) and (b-1), respectively. In Cell A, the carbon support for the Pt catalyst had a layered graphite-like structure with a lattice spacing of 0.34 nm. However, in Cell E, it appeared to have become amorphous during the long-term test, possibly due to oxidation of the carbon.

In order to determine whether there is any direct correlation among the growth of Pt particles, oxidation of the carbon support and the decline in the cell voltage, EPMA observations were conducted on cross sections of the MEAs from Cells A, C, D and E.

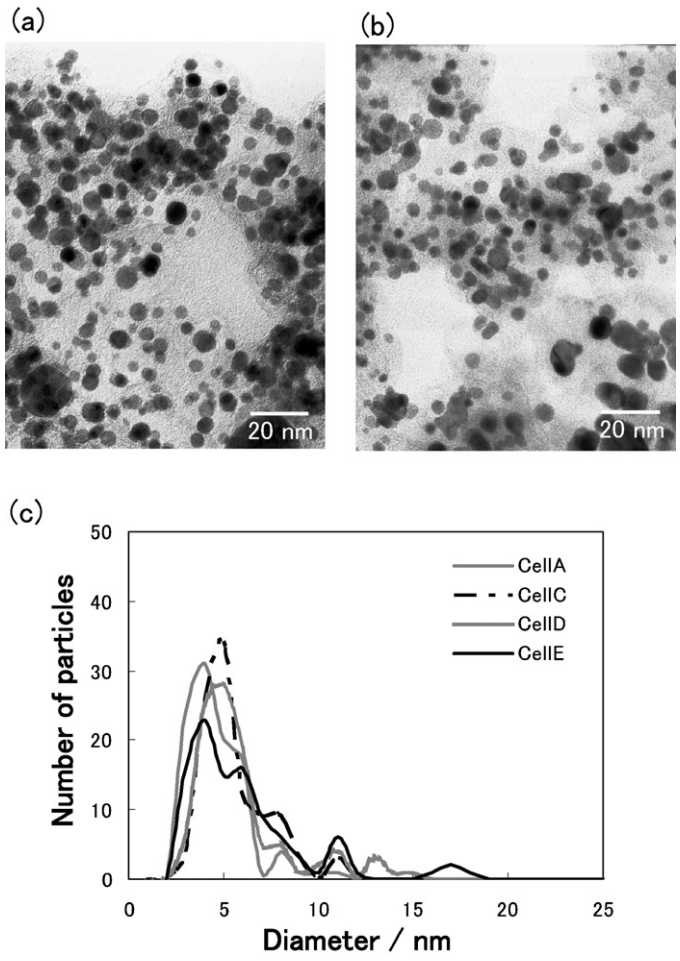

Fig. 4. Comparison of anode catalysts. (a) TEM image of anode catalyst of Cell A (0 h), (b) TEM image of anode catalyst of Cell E (17860 h), and (c) size distributions of anode Pt catalyst particles.

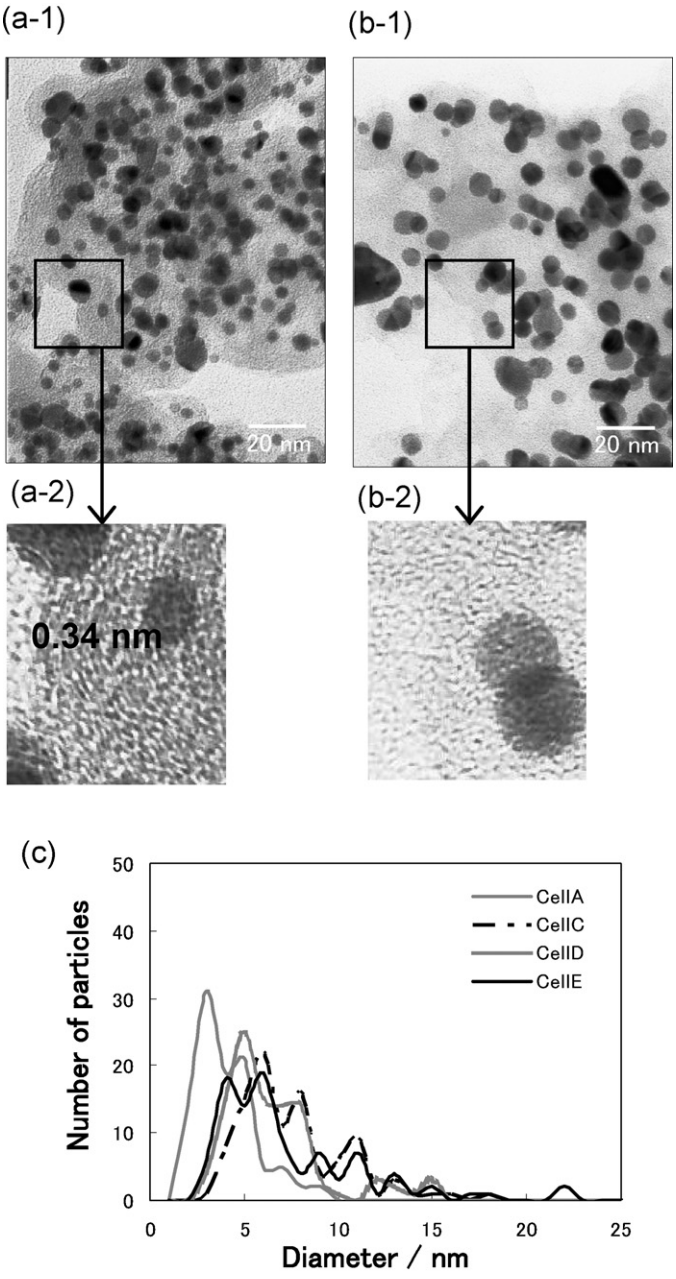

Fig. 5. Comparison of cathode catalysts. (a-1) TEM image of cathode catalyst of Cell A (0 h), (a-2) magnified image of (a-1), (b-1) TEM image of cathode catalyst of Cell E (17,860 h), (b-2) magnified image of (b-1), and (c) size distributions of cathode Pt catalyst particles.

3.4. EPMA observation of MEA cross sections

Figs. 6(a), 5(b), 6(c) and (d) show the Pt distributions determined by EPMA for cross sections of MEAs from Cells A, C, D and E, respectively. As shown in Fig. 6(a), the Pt concentration was initially highly uniform in both the anode and cathode catalyst layers. However, as shown in Fig. 6(b), following 12,000 h of operation, the Pt concentration in the circled areas became slightly higher than that in other areas. Furthermore, as shown in Figs. 6(c) and (d), this trend continued as the power generation time increased. Particularly high localized Pt concentrations were observed in both catalyst layers in Cell E following 17,860 h of operation. In addition, the catalyst layers, as a whole, became thinner with increasing power generation time. Fig. 6(e) and (f) shows the change in the thickness of the anode and cathode catalyst layers, respectively, as a function of testing time. The data points correspond to an average of fifty thickness measurements, and the errors bars represent the range of variations among the measurements. It can be seen that for both catalyst layers, the average thickness decreases, which correspond to the whole thickness reductions, roughly linearly with time.

Fig. 7(a)–(d) shows SEM images of cross sections of the MEAs from Cells A, C, D and E, respectively. It can be seen that the membrane thicknesses also decreases with increasing power generation time. This change in thickness is plotted in Fig. 7(e), where the data points are again averaged over fifty measurements and the range of variations is shown as error bars. The membrane thickness is seen to decrease very gradually over a period of about 14,000 h, after which it decreases more dramatically. These results are in good agreement with the decrease in cell voltage during the long-term power tests, as seen in Figs. 2 and 3.

Fig. 8(a)–(d) shows the phosphorus distributions determined by EPMA for cross sections of MEAs from Cells A, C, D and E, respectively. It is thought that these correspond to the phosphoric acid distributions. As seen Fig. 8(a), the initial phosphorus concentration was very low in both catalyst layers in Cell A. However, Fig. 8(b) shows that following 12,000 h of power generation, it increased substantially, indicating that migration of phosphoric acid from the membrane occurred. The phosphoric acid appears to be uniformly distributed in both catalyst layers.

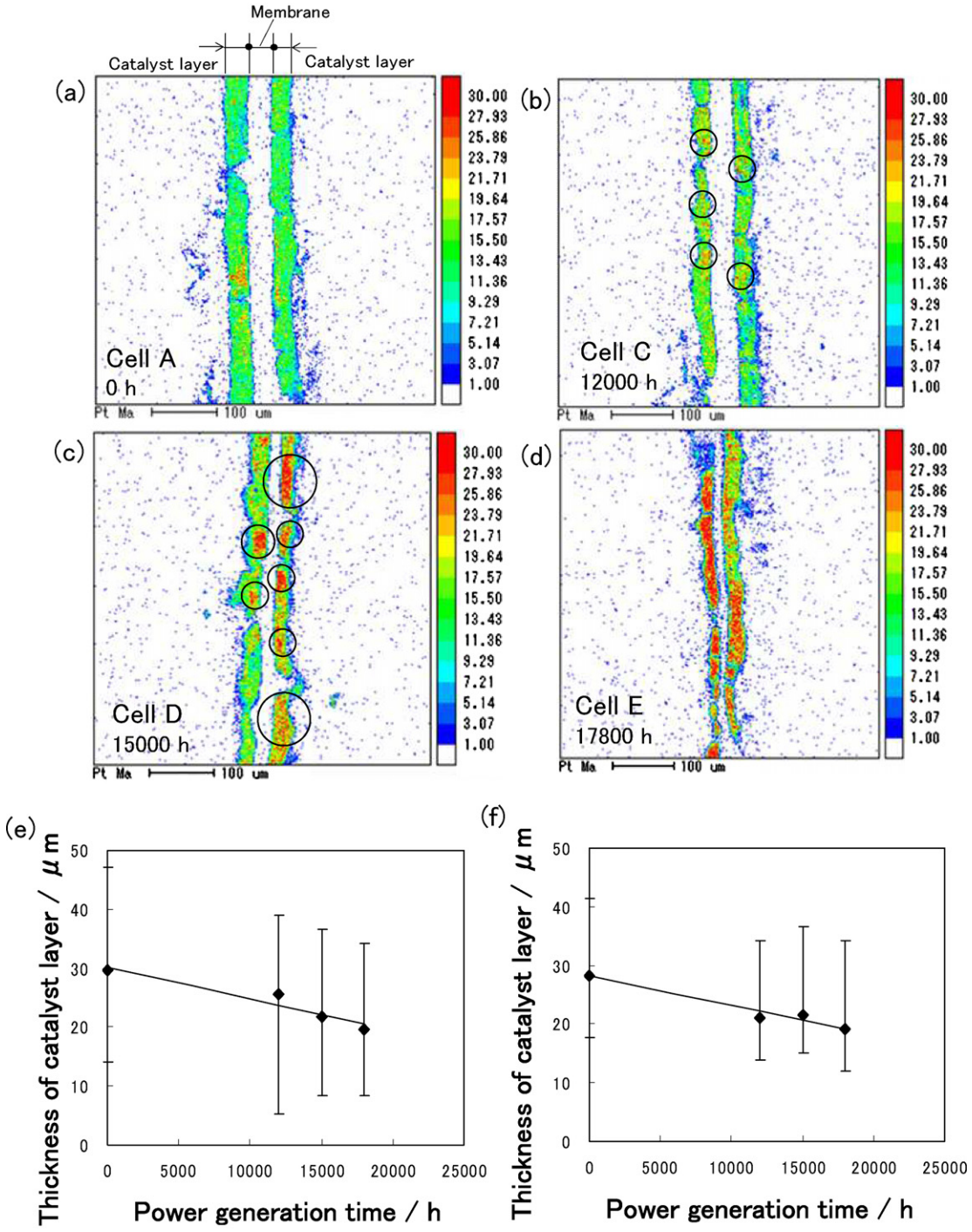

Fig. 6. EPMA Pt concentration analysis for cross sections of MEAs. (a) Pt concentration distribution in Cell A (0 h), (b) Pt concentration distribution in Cell C (12,000 h), (c) Pt concentration distribution in Cell D (15,000 h), (d) Pt concentration distribution in Cell E (17,860 h), (e) change in anode catalyst layer thickness with time, and (f) change in cathode catalyst layer thickness with time.

Following 15,000 h of operation, as shown in Fig. 8(c), this distribution became non-uniform and regions depleted of phosphoric acid began to appear in both catalyst layers. Such depletion of phosphoric acid would lead to a reduction in the active area of the Pt catalysts, and corresponds to the period following 14,000 h of operation when an accelerated decrease in the cell voltage occurs. Finally, as indicated by the circles in Fig. 8(d), following 17,860 h of power generation, a further increase in the number of depleted regions occurred, accompanied by rapid thinning of the membrane.

In order to evaluate the impact of membrane thinning and phosphoric acid migration on the cross leakage, leakage currents were measured for Cells C, D and E.

3.5. Measurement of leakage current

Fig. 9 shows the increase in the leakage current with time for Cells C, D and E. The relationship is seen to be logarithmic, with a very large leakage current occurring after 17,860 h of operation.

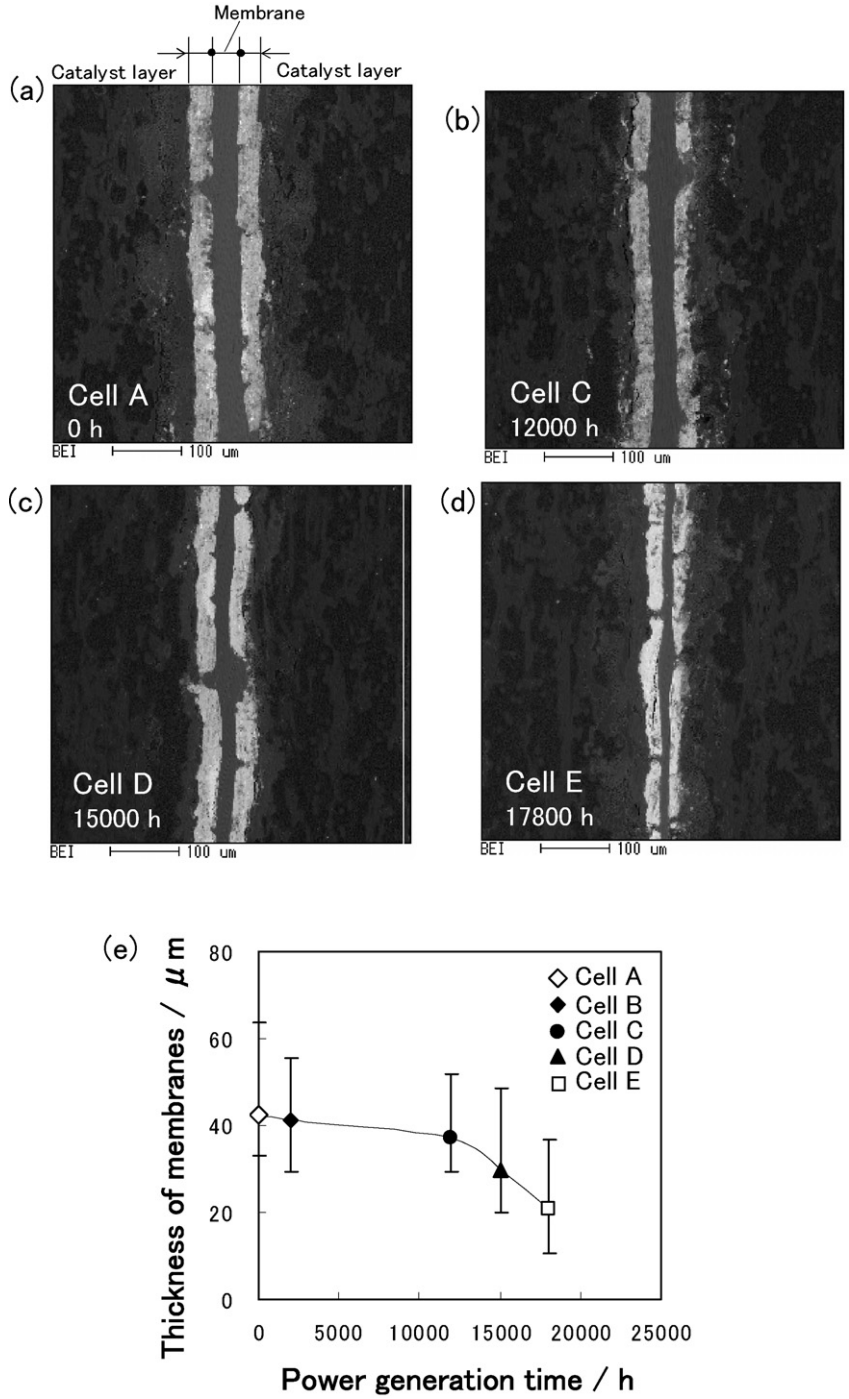

Fig. 7. EPMA of cross sections of MEAs. (a) SEM image of Cell A (0 h), (b) SEM image of Cell C (12,000 h), (c) SEM image of Cell D (15,000 h), (d) SEM image of Cell E (17,860 h), and (e) change in membrane thickness with time.

4. Discussion

4.1. Influence of Pt catalyst and carbon support degradation on cell voltage drop

From in Fig. 5(a-2) and (b-2), following 17,860 h of operation, it seems that the carbon support changed from having a layered graphite-like structure to an amorphous structure. Furthermore, the EPMA results shown in Fig. 6 indicate that both the anode and cathode catalyst layers became thinner as a linear function of power generation time, and their Pt particles became agglomerated. These results suggest that a large amount of the carbon support became oxidized and was removed as carbon dioxide. However, taking into account the linear dependence of the catalyst layer thinning on the power generation time, it is unlikely that carbon oxidization was responsible for the enhanced drop in the cell voltage that was observed from about 14,000 h.

On the other hand, since smaller catalyst particles are likely to agglomerate more easily, particle growth is expected to be more rapid in the early stages of power generation. This makes it unlikely that such particle growth was responsible for the enhanced drop in the cell voltage in the later stages of operation. In fact,

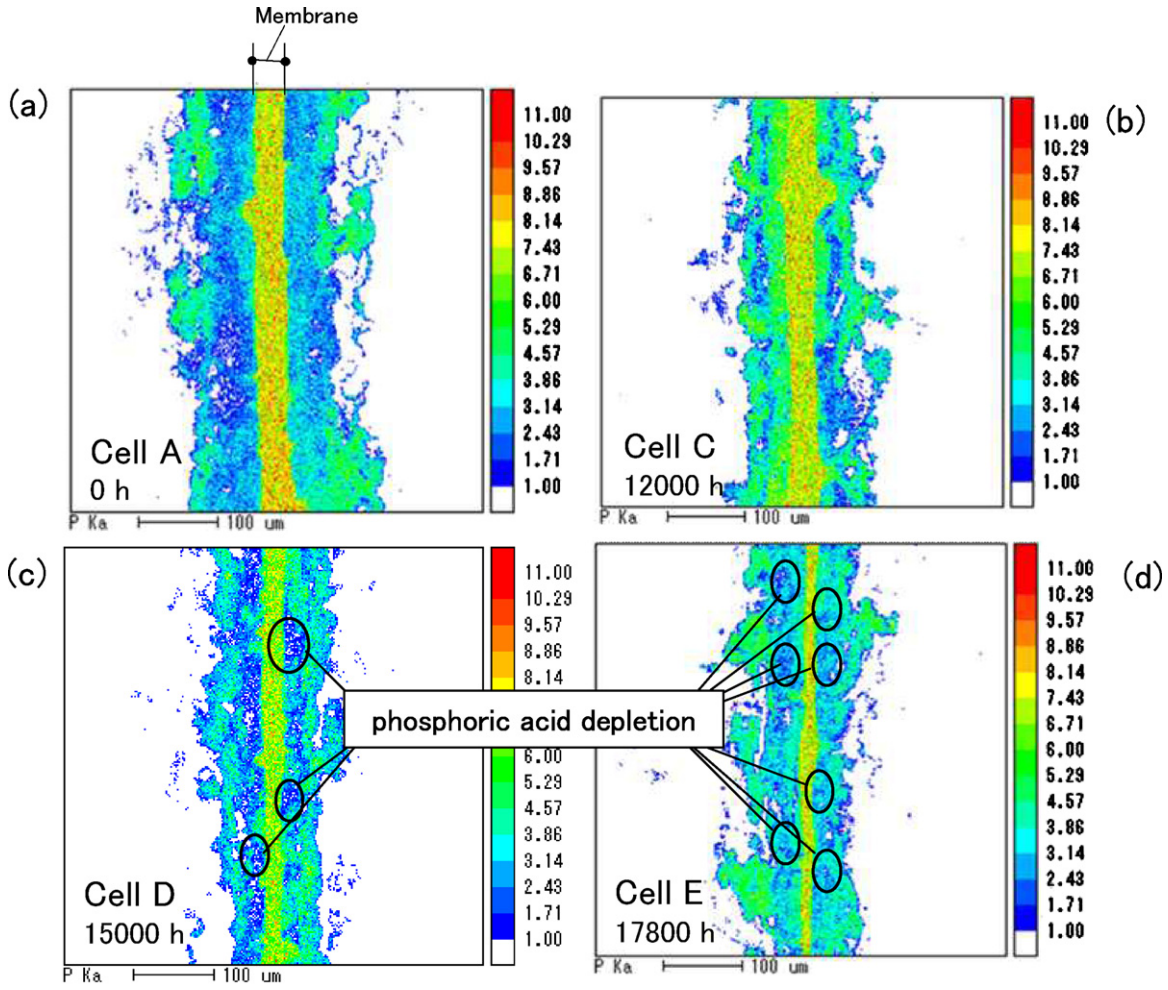

Fig. 8. EPMA phosphorus concentration analysis for cross sections of MEAs. (a) EPMA image of Cell A (0 h). The concentration of phosphoric acid is very low in both catalyst layers; (b) EPMA image of Cell C (12,000 h). A large amount of phosphoric acid is distributed uniformly in the catalyst layers; (c) EPMA image of Cell D (15,000 h). Depletion of phosphoric acid is observed in the catalyst layers; (d) EPMA image of Cell E (17,860 h). Increased number of phosphoric acid depleted regions observed in addition to membrane thinning.

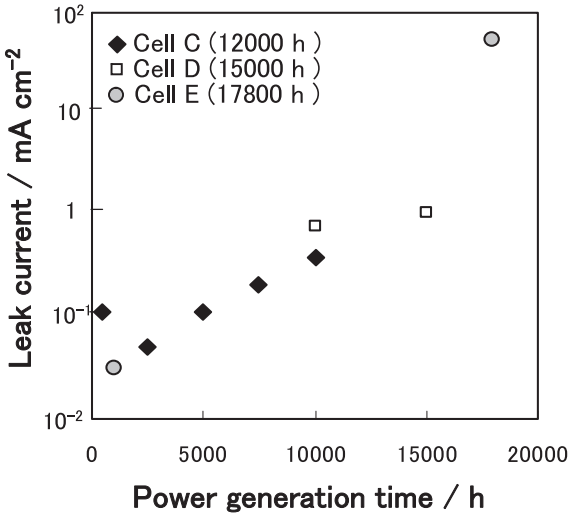

Fig. 9. Change in leakage current with time for Cells C, D and E.

growth of Pt catalyst particles during power generation at 150 °C has been reported within a relatively short period of approximately 500 h [21]. In addition, Zhai et al. reported that Pt aggregation occurs in the early stages of power generation and reduces the cell performance due to a reduction in the specific surface area of the Pt particles and an increase in the reaction resistance [21]. Considering these results, the reduction in cell voltage of approximately 20 mV in the initial stage of the durability test is considered to be caused by Pt particle growth [28].

4.2. Influence of membrane degradation on cell voltage drop

As shown in Fig. 7, the membrane thickness decreased very gradually up to about 14,000 h, and thereafter more rapidly, which is similar to the behavior of the cell voltage. As a result, the leakage current also increased, which is thought to have accelerated the degradation process. Furthermore, as shown in Fig. 9, local depletion of phosphoric acid occurred in both the anode and cathode catalyst layers, resulting in a reduction in the active areas of the catalyst layers.

In order to verify the correlation between membrane thinning and phosphoric acid depletion, the distributions of phosphorus and nitrogen were determined using EPMA. The phosphorus is associated with phosphoric acid whereas nitrogen is a constituent element of the PBI membrane, and its presence in the catalyst layers would therefore indicate dissolution of the membrane.

Fig. 10(a) and (b) shows the distributions of phosphorus and nitrogen, respectively, in the MEA from Cell E. The circles

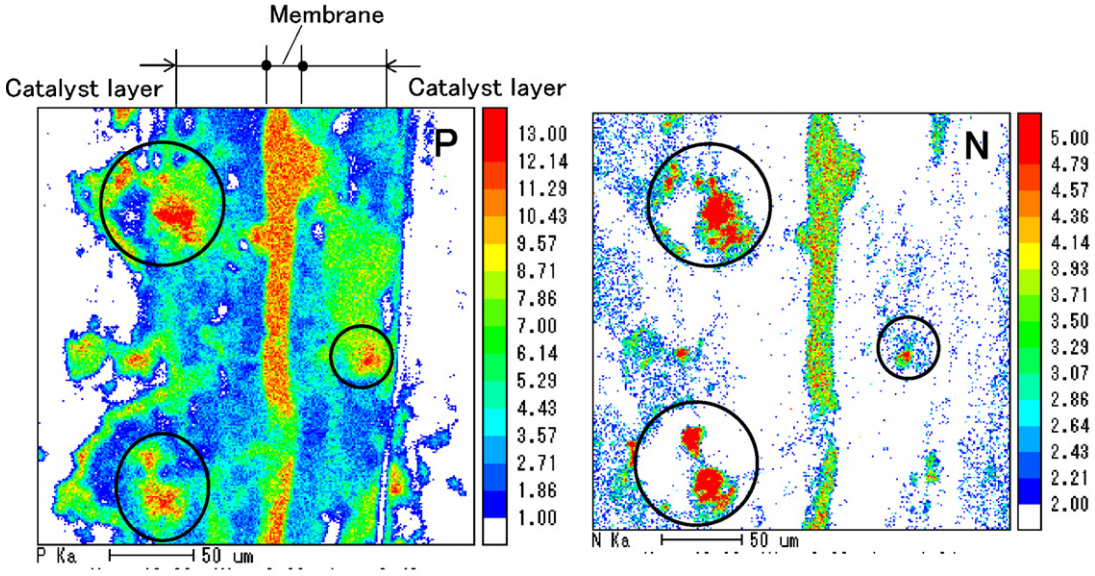

Fig. 10. EPMA of cross sections of MEAs from Cell E (17,860 h). (a) Phosphorus distribution, and (b) nitrogen distribution.

indicate regions where the concentrations of both phosphorus and nitrogen in the catalyst layers are high. This suggests that large regions of the membrane were dissolved during power generation and, together with the phosphoric acid, migrated into the catalyst layers. The migration led to large areas of the catalyst layers being depleted of phosphoric acid, resulting in a reduction in the active area. This is thought to be the reason for the accelerated drop in the cell voltage following 14,000 h of operation.

The membrane used in this study was not chemically bridged, which is thought to lead to the dissolution of membrane and finally its fragmented moieties. Higher durability is expected by using a bridged membrane.

5. Conclusion

For HT-PEMFCs using PBI membranes doped with phosphoric acid, five identical single cells were prepared and long-term power generation tests were conducted at a temperature of 150 °C and a current density of 0.2A cm^{-2} for periods of up to 17,860 h. Following the tests, the MEAs from the cells were analyzed using TEM and EPMA.

The results indicated that the cell voltage declined very gradually until 14,000 h, after which a more rapid decrease occurred. The former was guessed to be caused by the active area decrease due to catalyst agglomeration and so on. And the latter was found to correlate well with decreases in the membrane thickness. It was also found that parts of the membrane became dissolved and migrated together with the phosphoric acid into the catalyst layers. Regions of the catalyst layers that were depleted of phosphoric acid were identified, which resulted in a reduction in the active area, which is thought to be the cause of the accelerated drop in the cell voltage after about 14,000 h of operation.

References

[1] T. Shimizu, 7th Int'l Hydrogen & Fuel Cell Expo, FC-4, 2011, p. 18.
[2] P. Krishnan, J.S. Park, C.S. Kim, J. Power Sources 159 (2006) 817.
[3] H. Xu, Y. Song, H.R. Kunz, J.M. Fenton, J. Power Sources 159 (2006) 979.
[4] C.P. Wang, H.S. Chu, Y.Y. Yan, K.L. Hsueh, J. Power Sources 170 (2007) 235.
[5] J. Karstedt, J. Ogrzewalla, C. Severin, S. Pischinger, J. Power Sources 196 (2011) 9998.
[6] D. Plackett, A. Siu, Q. Li, C. Pan, C. Pan, J.O. Jensen, A.A. Permyakova, N.J. Bjerrum, J. Membr. Sci. 383 (2011) 78.
[7] J. Lobato, P. Canizares, M.A. Rodrigo, D. Ubeda, F.J. Pinar, J. Lobato, P. Canizares, M.A. Rodrigo, D. Ubeda, F.J. Pinar, J. Membr. Sci. 369 (2011) 105.
[8] J. Hu, J. Luo, P. Wagner, O. Conrad, C. Agert, Electrochem. Commun. 11 (2009) 2324.
[9] R. Bouchet, E. Siebert, Solid State Ionics 118 (1999) 287.
[10] B. Xing, O. Savadogo, Electrochem. Commun. 2 (2000) 697.
[11] P. Donoso, W. Gorecki, C. Berthier, F. Defendini, C. Poinsignon, M. Armand, Solid State Ionics 28–30 (1988) 969.
[12] M.S. Boroglu, S.U. Celik, A. Bozkurt, I. Boz, J. Power Sources 375 (2011) 157.
[13] S. Zeng, L. Ye, S. Yan, G. Wu, Y. Xiong, W. Xu, J. Power Sources 367 (2011) 78.
[14] D. Rogriguez, C. Jegat, O. Trinquet, J. Grondin, J.C. Lassègues, Solid State Ionics 61 (1993) 195.
[15] M.F. Daniel, B. Desbat, F. Cruege, O. Trinquet, J.C. Lassègues, Solid State Ionics 28–30 (1988) 637.
[16] J.A. Asensio, S. Borros, P.G. Romero, J. Electrochem. Soc. 151 (2004) A304.
[17] J.R.P. Jayakody, S.H. Chung, L. Durantio, H. Zhang, L. Xiao, B.C. Benicewicz, S.G. Greenbaum, J. Electrochem. Soc. 154 (2007) B242.
[18] Q. Li, J.O. Jensen, R.F. Savinell, N.J. Bjerrum, Prog. Polym. Sci. 34 (2009) 449.
[19] J. Parrondo, F. Mijangos, B. Rambabu, J. Power Sources 195 (2010) 3977.
[20] J. Lobato, P. Canizares, M.A. Rodrigo, F.J. Pinar, D. Ubeda, J. Power Sources 196 (2011) 196.
[21] Y. Zhai, H. Zhang, D. Xing, Z.G. Shao, J. Power Sources 164 (2007) 126.
[22] J. Zhang, Y. Tang, C. Song, J. Zhang, J. Power Sources 172 (2007) 163.
[23] A. Sounai, K. Sakai, Proceedings of the 13th Fuel Cell FCDIC Symposium, 2006, p. 125.
[24] J. Baurmeister, T. Kohno, Proceedings of the 13th Fuel Cell FCDIC Symposium, 2006, p. 122.
[25] Y. Oono, A. Sounai, M. Hori, J. Power Sources 189 (2009) 943.
[26] J. Yu, Y. Yoshikawa, T. Matsuura, M.N. Islam, M. Hori, Electrochem. Solid-State Lett. 8 (3) (2005) A152.
[27] J. Yu, T. Matsuura, Y. Yoshikawa, M.N. Islam, M. Hori, Electrochem. Solid-State Lett. 8 (3) (2005) A156.
[28] Y. Oono, T. Fukuda, A. Sounai, M. Hori, J. Power Sources 195 (2010) 1007.
[29] I. Okae, S. Kato, A. Seya, T. Kamonoshita, The Chemical Society of Japan 67th Spring Meeting, 1990 p. 148.